Cellular Signalling 60 (2019) 122–135

Contents lists available at ScienceDirect

Cellular Signalling

journal homepage: www.elsevier.com/locate/cellsig

Knockdown of cZNF292 suppressed hypoxic human hepatoma SMMC7721 cell proliferation, vasculogenic mimicry, and radioresistance

Wei Yang[a,*], Yingying Liu[a,b], Ruoling Gao[a], Zenghe Xiu[a], Ting Sun[c,d,**]

[a] State Key Laboratory of Radiation Medicine and Protection, School of Radiation Medicine and Protection and Collaborative Innovation Center of Radiation Medicine of Jiangsu Higher Education Institutions, Soochow University, Suzhou, Jiangsu, China
[b] Isotopic Laboratory of Nuclear Medicine, Xi'an Central Hospital, Xi'an, Shaanxi, China
[c] Neurosurgery and Brain and Nerve Research Laboratory, The First Affiliated Hospital of Soochow University, Suzhou, Jiangsu, China
[d] Division of Surgical Oncology, Massachusetts General Hospital, Harvard Medical School, Boston, MA, USA

ARTICLE INFO

Keywords:
circRNA ZNF292
SOX9
β-catenin
Hypoxia
Radioresistance

ABSTRACT

Hypoxia is a classic feature of the tumor microenvironment, and has been established as a key epigenetic factor modulating the outcome of radiotherapy. Circular RNAs (circRNAs) are novel RNA molecules with covalently closed circular structures and are highly expressed in eukaryotic transcriptomes. Although previous analysis have shown that circRNA ZNF292 (cZNF292) was hypoxia-responsive and exhibited a proangiogenic function in vitro, the molecular mechanism of cZNF292's biological function is still unclear and deserves further exploration. In this study, we investigated the effect of cZNF292 on the vasculogenic mimicry (VM) and radiosensitivity of hypoxic hepatoma SMMC7721 cells and its mechanism. Our data indicated that cZNF292 could be induced by hypoxia in a time-dependent manner in hepatoma cells independent of hypoxia inducible factor (HIF)-1α. Knockdown of cZNF292 increased SRY (sex determining region Y)-box 9 (SOX9) nuclear translocation, subsequently reduced Wnt/β-catenin pathway activity, leading to suppression of hypoxic hepatoma cell proliferation, VM, and radioresistance in vitro and in vivo. Our results delineated a novel mechanism of cZNF292 in enhancing hypoxic tumor cell radiosensitivity, which might provide valuable targets for radiation therapy for hepatoma.

1. Introduction

Liver cancer was the sixth most common-incident cancer worldwide and the fourth most common cause of cancer death [1]. There were 854,000 incident liver cancer cases and 810,000 deaths globally in 2015, contributing to 20,578,000 disability-adjusted life-years (DALYs). The highest burden of liver cancer incident cases, deaths, and DALYs was observed in East Asia [2]. The most common type of primary liver cancer globally is hepatocellular carcinoma (HCC) [3,4]. At present, the treatment of HCC mainly includes surgical resection, chemotherapy and radiotherapy. Ionizing radiation is a widely used treatment method for HCC patients, but it also has certain limitations and imperfections [5,6]. Thus, it is extremely important to actively improve the effectiveness of radiotherapy.

Most of the solid tumors have hypoxic regions, including HCC, because rapid cell growth within tumors leads to insufficient vascularization [7,8]. However, tumor cells can activate a wide range of transcription factors, such as hypoxia-inducible factor-1α (HIF-1α), which control multiple cellular functions critical in cancer progression, including metabolism, angiogenesis, extracellular matrix remodeling, cell proliferation and survival, reactive oxygen species (ROS) homeostasis and so on [9–11]. Notably, the hypoxic microenvironment makes cancer cells more resistant to radiotherapy and become a hidden danger of tumor recurrence and metastasis [12–14].

At the molecular level, scholars have paid more and more attention to the role of non-coding RNAs (ncRNAs) in human diseases or life processes [15,16]. In recent years, a new star, circular RNA (circRNA), has been discovered in the field of ncRNAs. It is a covalently closed circular structural RNA formed by its parental linear gene by means of splicing, and has neither 5′-3′ polarity nor polyA tail [17,18]. Studies have found that circRNAs, similar to other non-coding RNAs, are involved in regulating various life processes and can be used as biomarkers for diagnosing or predicting diseases [19–21]. Memczak et al. found a variety of circRNAs specifically expressed in different cell types or developmental stages (1950 circRNAs in humans, 1903 circRNAs in mice, and 724 circRNAs in *C. elegans*) [22]. Furthermore, recent studies

* Correspondence to: W. Yang, 199 Renai Road, Suzhou, Jiangsu 215123, China.
** Correspondence to: T. Sun, 708 Renmin Road, Suzhou, Jiangsu 215006, China.
E-mail addresses: detachedy@aliyun.com (W. Yang), sunting1979st@aliyun.com (T. Sun).

https://doi.org/10.1016/j.cellsig.2019.04.011
Received 29 January 2019; Received in revised form 21 April 2019; Accepted 23 April 2019
Available online 24 April 2019
0898-6568/

found that circRNAs played an important role in cancer development, regulating cancer metabolism, apoptosis, proliferation, migration and so on [23–25].

Boeckel et al. explored the expression and function of circRNAs in endothelial cells and characterized hypoxia-controlled endothelial circRNAs and showed that cZNF292, cAFF1, and cDENND4C were up-regulated, whereas cTHSD1 was reduced, by hypoxia [26]. One of the highly expressed and significantly regulated circRNAs, cZNF292, exhibited a proangiogenic function in vitro. The authors further explored the mechanism by which cZNF292 controls angiogenic functions. Surprisingly, they found that cZNF292 had neither cis-regulatory function on host gene expression, nor a putative function as an miRNA sponge [26]. Until now, the molecular mechanism of cZNF292's biological function is still unclear and deserves further exploration.

In this study, we investigated the function of cZNF292 on the vasculogenic mimicry (VM) and radiosensitivity of hypoxic hepatoma cells and its mechanism. Our data indicated that cZNF292 could be induced by hypoxia in a time-dependent manner in hepatoma cells independent of HIF-1α. Knockdown of cZNF292 increased SRY (sex determining region Y)-box 9 (SOX9) nuclear translocation, subsequently reduced Wnt/β-catenin pathway activity, leading to suppression of hypoxic hepatoma cell proliferation, VM, and radioresistance. Our data will shed new light on the potential role of cZNF292 in hypoxic tumor cells and its possible molecular mechanisms.

2. Materials and methods

2.1. Cell culture

Human hepatocellular carcinoma SMMC7721 cells were maintained in Dulbecco's Modified Eagles Medium (DMEM) (Hyclone, China) supplemented with 10% fetal bovine serum (FBS) (BC, Australia) in a humidified atmosphere containing 5% CO2 at 37 °C. Cells treated with hypoxia were exposed to a steady flow of low-oxygen gas mixture (1% O2, 5% CO2, 94% N2) in a modular incubator chamber (MiniGalaxy, RSBiotech, Irvine, Scotland).

2.2. RNA isolation and RT-PCR

Total RNA was extracted from cultured cells with Trizol (Ambion, USA) and cDNA was generated using the First Strand cDNA Synthesis kit (TaKaRa, China). Expression level of circRNAs and mRNAs were analyzed using the SYBR Green PCR Master Mix (TaKaRa, China) on a 7500 Real-Time PCR System (Applied Biosystems, USA). Fold changes in circRNAs and mRNAs expression were normalized to the housekeeping gene RPLP0 by using the $2^{-\Delta\Delta CT}$ relative quantification method. Primers used for qRT-PCR were as follows: cZNF292 forward, 5′-GCT CAAGAGACTGGGGTGTG-3′ and reverse, 5′-AGTGTGTGTTCTGGGGC AAG-3′. cDENND4C forward, 5′-CTTCATGACCCACCACAAGATG-3′ and reverse, 5′-GGGTGTGGCTAGGATCACTTC-3′. cAFF1 forward, 5′-GCCA AGCT CACCAAACTGAA-3′ and reverse, 5′-CCTGGTTGCGTCTTTCC TTC-3′. cTHSD1 forward, 5′-CTACATGGCCTGGCTCTCTC-3′ and reverse, 5′-AGTACTGCTTT GACTTTGGCA-3′. ZNF292 forward, 5′-GCAA AGCTGTGTTCTGACCA-3′and reverse, 5′-CTTGTTGGAGCTGACGT GAC-3′. RPLPO forward, 5′-TCGACAATG GCAGCATCTAC-3′ and reverse, 5′-ATCCGTCTCCACAGACAAGG-3′.

2.3. siRNA design and transfection

The cDNA sequences of HIF-1α and SOX9 were obtained from GenBank (NM-001530 and 000346.3). The siRNA target design tools from Ambion were used to design siRNA. HIF-1α-siRNA was designed and synthesized as follows: sense: 5′- CCUCAGUGUGGGUAUAAG ATT-3′, antisense: 5’-UCUUAUACCCACACUGAG GTT-3′. SOX9-siRNA was designed and synthesized as follows: sense: 5′- AGCCCGAUCUGA AGAAGGATT-3′, antisense: 5′-UCCUUCUUCAGAUCGGG CUCG-3′ (Sangon Inc. Shanghai, China). Cells were plated 24 h prior to transfection and were transfected in 6-well plates by use of Lipofectamine RNAiMAX (Invitrogen, Carlsbad, CA, USA). HIF-1α and SOX9-siRNA and negative control siRNA were used at 100 nM final concentration.

2.4. Lentivirus vector construction and transduction

Recombinant lentivirus vector harboring shRNA sequences targeting human cZNF292 (Lv-sh-cZNF292) and recombinant control lentivirus vector (Lv-sh-ctrl) were constructed by GenePharma, Shanghai. The shRNA sequences targeting cZNF292 were as follows: 5′-CAGAACACACACTATAGAG-3′. The random shRNA sequences were as follows: 5′-TTCTCCGAACGTGTCACGT-3′. The cells were cultured in 24-well plates. When the cell confluence rate reached 60%, lentivirus were added to culture medium. The final concentration of 5 μg/ml polybrene was added to enhance the transduction efficiency. Stably transfected cells were selected with puromycin at a final concentration of 1 μg/ml for 4 weeks.

2.5. Proliferation assay

Cells were seeded into 96-well plates. After 12, 24, 36, 48 h incubation under normoxic or hypoxic conditions, 10 μl CCK8 reagent (DOJINDO, China) was added into each well and incubated for 2 h at 37 °C in the dark. The optical density (OD) value per well was measured at 450 nm with a multi-functional microplate reader (BioTek, USA).

2.6. Flow cytometric analysis of cell cycle and apoptosis

Cells were harvested and immediately fixed with 75% ethanol and stored at −20 °C. Cells were stained in staining buffer (10 μg/ml PI and 100 μg/ml RNase A) (Bi Yuntian, China) for 30 min at 37 °C and then analyzed on a flow cytometer Beckton Dickinson (*BD*) *FACScan* (*BD* Biosciences, San Jose, CA).

Quantification of apoptotic cells was performed according to the Annexin-V-PE/7-AAD Apoptosis Detection Kit manufacturer instructions (KeyGen BioTECH, China). Analyses were performed by a flow cytometer (BD FACScan). Phycoerythrin (PE)-positive and 7-amino-actinomycin D (7-AAD)-negative cells were regarded as apoptotic cells.

2.7. 3D VM formation

Matrigel (Collaborative Biomedical) (Corning, USA) was thawed at 4 °C, and 200 μl of Matrigel was rapidly added to each well of a 24-well plate, allowed to solidify for 1 h at room temperature, and placed at 37 °C in a humidified 5% CO_2 incubator for 30 min. Tumor cells were seeded in complete medium in Matrigel-coated wells, and incubated in normoxic or hypoxic (1% O_2) condition at 37 °C for different time [26].

2.8. Western blot analysis of protein expression

Western blotting was performed using standard procedures. The following primary antibodies were used: mouse monoclonal anti-HIF-1α, ZNF292, β-catenin, CyclinD1, c-Myc, p21, Twist1, vascular endothelial cadherin (VE-cadherin), DNA-dependent protein kinase catalytic subunit (DNA-PKcs) (S2056), ataxia telangiectasia mutated (ATM) (S1981), SOX9 and β-actin (Cell Signaling, USA). Experiments were repeated three times. The relative levels of protein expression were normalized against protein levels of an internal control gene, β-actin, performed in the same run.

2.9. Colony formation assay

Pretreated cells from the cZNF292 knockdown groups and the negative control groups were seeded into 3.5 cm culture dishes. The cells were exposed to 0, 2, 4, 6, and 8 Gy X-ray (160 KV) at room

temperature using a linear accelerator (RadSource, Suwanee, GA, USA) at a dose rate of 1.15 Gy/min. After irradiation, control and irradiated cells were incubated for 12 days. Then colonies were fixed and stained with 0.1% crystal violet. Colonies containing > 50 cells were counted. Furthermore, the cell survival fraction was counted out and the mean lethal dose (D_0) was calculated by the linear quadratic model. The colony formation assay was repeated at least 3 times.

2.10. Immunofluoresence staining for γH2AX-foci

Cells were stained with primary antibody for γH2AX (Epitomics, Burlingame, CA, USA) and slides were incubated for 1 h with Alexa-488-conjugated anti-rabbit IgG for visualization of foci. Fluorescence analyses were performed with a DM 6000 B microscope (Leica, Germany). Every microscope slide was counted at least three times by two blinded observers independently. In order to get the x-ray induced γH2AX-foci (so-called excess γH2AX-foci), we subtracted the absolute γH2AX-foci before irradiation (so-called background foci) from the absolute γH2AX-foci after exposure [27].

2.11. DNA-PKcs kinase assay

DNA-PKcs kinase activity was measured with the SigmaTECT DNA-PK Assay System (Promega) following the manufacturer's instruction. After [γ-32P]-ATP isotope labelling of the phosphorylation products and removal of non-specific signals by washing, the SAM2® Membrane squares were subjected to scintillation counting.

2.12. RNA binding protein immunoprecipitation (RIP)

In brief, 10^7 hypoxic cells were washed in ice-cold PBS, lysed in 500 μl co-IP buffer and incubated with 5 μg of primary antibody (anti-mouse IgG, β-catenin, APC, Axin, SOX6, SOX9, SOX17, and HIF-1α) at 4 °C for 2 h. A total of 40 μl of 50% slurry of protein A-Sepharose was added to each sample, and the mixtures were incubated at 4 °C for 4 h. The pellets were washed with PBS and resuspended in 0.5 ml Tri Reagent (Sigma-Aldrich). The eluted co-precipitated RNA in the aqueous solution was subject to qRT-PCR analysis to demonstrate the presence of the binding products using respective primers [28].

2.13. RNA pull-down assays

After 10^7 hypoxic control and cZNF292 knockdown cells were washed in pre-chilled PBS, they were lysed in 500 μl Co-IP buffer and mixed with 3 μg biotinylated DNA oligonucleotides probes (5′-biotin-AGTGTGTGTTCTGGGGCAAGCCTTTATCCTT ATCCAATGG-3′, Biotium, USA) against cZNF292 at room temperature for 2 h. A total volume of 50 μl of streptavidin C1 magnetic beads (Invitrogen) were added to each conjugate for reaction and further incubated at room temperature for 1 h. The beads were briefly washed five times with Co-IP buffer. The bound proteins in the pull-down complex were analyzed by Western blot [28].

2.14. Subcellular fractionation

Cells were homogenized in hypotonic buffer (10 mM Tris-HCl, pH 7.8, 150 mM NaCl, and 1 mM EDTA) containing 0.1% (*w/v*) Triton X-100. The lysates were centrifuged at 3000 rpm for 10 min at 4 °C. The pellet was re-suspended in hypotonic buffer and re-centrifuged and was used as the nuclear fraction. The supernatant fraction was re-centrifuged at 16,000 rpm for 20 min at 4 °C and used as the cytoplasmic fraction [28].

2.15. Immunofluorescent microscopy

Cells growing on BD culture slides were fixed in 3.7% formaldehyde for 10 min, blocked with 10% goat serum for 30 min, and then incubated with primary antibody in TBS containing 10% goat serum albumin overnight. The slides were washed and stained with goat anti-mouse Alexa 488 (Life Technologies) at room temperature for 1 h. DNA staining was performed with DAPI. Confocal laser scanning microscopy was performed using an LSM 510 Meta microscope (Carl Zeiss) [29].

2.16. Fluorescent in situ hybridization (FISH)

FISH were used to detect cZNF292 expression within cells with a mixture of DNA oligo probes labelled with Cy5, which was specific for endogenous cZNF292. A scramble sequence labelled with Cy5 was used as a negative control. Cells growing on culture slides were fixed in 3.7% formaldehyde for 10 min, and then permeabilized with 0.2% Triton X-100 for 15 min. In situ Hybridization was carried out at 52 °C for 3 h with 40 nM Cy5-labelled DNA oligo probes in hybridization buffer (Ambion), followed by serial washes with saline-sodium citrate (SSC) buffers. The samples were treated with 3% hydrogen peroxide to block endogenous peroxidase, washed three times and then incubated in blocking buffer at room temperature for 30 min. DNA staining was performed with DAPI. Confocal laser scanning microscopy was performed using an LSM 510 Meta microscope (Carl Zeiss) [28].

2.17. β-catenin expression vectors construction and transfection

Full-length cDNA of β-catenin was isolated from cDNA of SMMC7721 cells and was amplified through RT-PCR using specific forward 5′-AAAATCCAGCGTGG ACAATGG-3′ and reverse, 5′-TGTGGC AAGTTCTGCATCATC-3′ primers. The amplified cDNA fragment was cloned into the pcDNA3.1(+) vectors. The recombinant vectors were confirmed by the digestion analysis of restriction endonuclease and inserted sequences were verified by DNA sequencing. Cells with stable integration of sh-cZNF292 were plated 24 h prior to transfection. Cells were transfected in 6-well plates by use of Lipofectamine 2000 (Invitrogen, Carlsbad, CA, USA).

2.18. Tumor-bearing mice model and treatment

For in vivo implantation, SMMC7721, SMMC/sh-ctrl and SMMC/sh-cZNF cells were washed in Hanks' balanced salt solution (HBSS) and injected subcutaneously at 1×10^6 cells in 0.1 ml HBSS in the right hind limb of 6–8-week-old female Balb/c nude mice (Experimental Animals Center of Shanghai Institute of Life Science, Shanghai, China), respectively. When the diameter of tumor reached about 6–8 mm, the mice implanted with SMMC7721 cells (14 days after inoculation) were taken as control and the mice implanted with SMMC/sh-ctrl (14 days after inoculation) or SMMC/sh-cZNF (20 days after inoculation) cells were randomly divided. The mice implanted with SMMC/sh-ctrl cells were divided into two groups: The negative control vector group received no X-irradiation; Radiotherapy group was subjected to 8 Gy (2 Gy/d for 4 successive days) X-ray irradiation (6 MV, the dose rate was 100 cGy/min) by a PRIMUS accelerator (SIEMENS Medical Solutions, Erlangen, Germany) at room temperature. The mice implanted with SMMC/sh-cZNF cells were divided into two groups: cZNF292 knockdown group received no X-irradiation; Combined therapy group was subjected to 8 Gy X-ray irradiation. Irradiation was locally confined to the tumors by shielding the rest of the body with lead and was conducted 1 day after dividing. Mice were monitored for tumor growth and survival. All the animal experiments were conducted in accordance with Guidelines for the Welfare of Animals in Experimental Neoplasia.

2.19. Immunohistochemical studies for Ki-67 in tumor tissues

The mice used for immunohistochemical studies were sacrificed 1 day after the irradiation. Tumor tissues were fixed and imbedded in

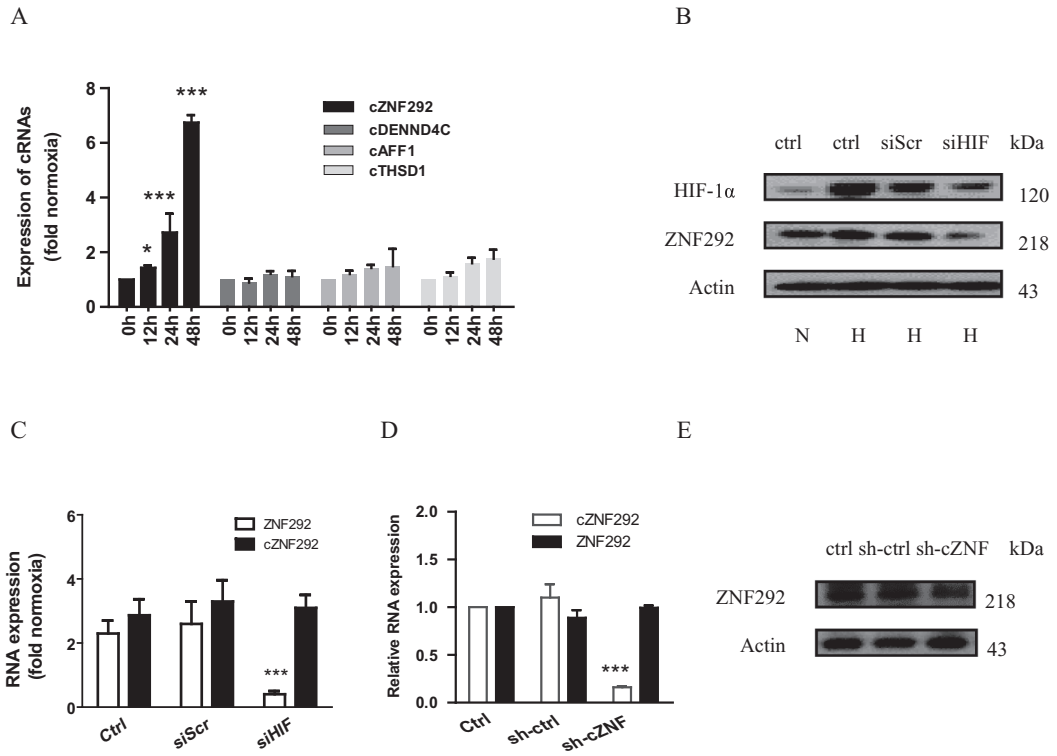

Fig. 1. cZNF292 was induced by hypoxia in hepatoma cells, and independent of hypoxia inducible factor (HIF)-1α. a Real-time RT-PCR detection of four circRNAs expression in hypoxic SMMC7721 cells. b HIF-1α and ZNF292 expression in SMMC7721 cells detected by western blot. c Real-time RT-PCR detection of cZNF292 and ZNF292 expression levels after HIF-1α knockdown in hypoxic SMMC7721 cells. d Real-time RT-PCR detection of cZNF292 and ZNF292 expression levels after cZNF292 knockdown in hypoxic SMMC7721 cells. e ZNF292 expression after cZNF292 knockdown in hypoxic SMMC7721 cells detected by western blot. Data are the means ± SEM of three experiments. *$p < .05$; ***$p < .001$.

paraffin. Tumor sections of 5 μm were cut from the imbedded tissue and incubated with specific primary antibodies, including rabbit monoclonal antibody to human Ki-67 (KeyGen Biotech.) for 1 h at 37 °C followed by overnight at 4 °C in humidity chamber. Negative controls were incubated only with universal negative control antibodies under identical conditions. The sections were then incubated with appropriate biotinylated secondary antibody for 60 min at room temperature. Thereafter, sections were incubated with conjugated horseradish peroxidase streptavidin (KeyGen Biotech.) for 60 min, followed with 3,3′-diaminobenzidine (Sigma) working solution, and counterstained with hematoxylin. The proliferation index was determined as number of Ki-67-positive (brown) cells/total number of cells × 100 in 9 most highly vascularized fields (400×).

2.20. CD31-PAS dual staining

Five micrometer paraffin sections were routinely deparaffinized and dehydrated. First, CD31 immunohistochemical staining was applied to the sections, using the immunohistochemistry method described above, with primary antibody: rabbit antimouse CD31 (1:200 eBioscience, Inc., San Diego, CA, USA). Sections were then treated with 0.5% periodic acid solution (PAS) for 10 min and rinsed with distilled water for 2–3 min. In a dark chamber, sections were treated with Schiff solution for 15–30 min. After rinses with distilled water, sections were counterstained with hematoxylin. Nine fields of vision of the phase contrast microscope of each pathological section were selected for counting of the number of endothelial-dependent vessels and VM at 400 × magnification. The average number of endothelial-dependent vessels (CD31-positive (brown) cells) and VM, which are quantification of the microvessel density (MVD) and the vasculogenic mimicry density (VMD) in tumors, were calculated [30].

2.21. Detection of apoptotic cells in tumor tissues

Apoptotic cells in tumor tissues were detected by terminal deoxynucleotidyl transferase (TdT)-mediated dUTP-biotin nick end labeling (TUNEL) stain, using an In Situ Cell Death Detection Kit (KeyGen Biotech.) following the manufacturer's specifications. In brief, tumor histological sections were permeabilized using a mixture containing 0.1% sodium citrate and 0.1% Triton X-100 and incubated with TUNEL reaction mixture containing terminal deoxynucleotidyltransferase and fluorescein-dUTP at 37 °C for 60 min. The apoptotic index was calculated as number of apoptotic (brown) cells/total number of cells × 100 in 9 randomly selected fields (400×).

2.22. Statistical analysis

All statistical parameters were calculated with GraphPad Prism 5.0 (GraphPad Software Inc.). Student's *t*-test was used for most data analysis. For comparisons among more than two groups, One-way Analysis of Variance (ANOVA) followed by Bonferroni post-test was performed. $p < .05$ was considered to be statistically different.

3. Results

3.1. cZNF292 was induced by hypoxia in a time-dependent manner in hepatoma cells, and independent of hypoxia inducible factor (HIF)-1α

To investigate whether the hypoxic-reactive circRNAs (cZNF292, cAFF1, cDENND4C, and cTHSD1) in endothelial cells were also regulated by hypoxia in tumor cells, we used real-time reverse transcription-polymerase chain reaction (RT-PCR) to detect the expression changes of the above four circRNAs in hepatoma cells exposed to 1% oxygen for 0, 12, 24 and 48 h. The results showed that only cZNF292 expression was

significantly induced by hypoxia and increased with hypoxic time. cAFF1, cDENND4C, and cTHSD1 expression showed no obvious changes in SMMC7721 cells upon hypoxic exposure (Fig. 1a). Cellular responses to hypoxia are commonly regulated by the hypoxia inducible factor family of transcriptional factors. To investigate whether the hypoxic-responsive cZNF292 was regulated by HIF-1α, we use siRNAs targeting HIF-1α to knockdown HIF-1α and detect the expression changes of cZNF292 in SMMC7721 cells after 48 h hypoxic incubation. Our results showed that HIF-1α knockdown significantly down-regulated mRNA and protein levels of ZNF292, a target gene of HIF-1α (Fig. 1b,c). However, cZNF292 expression showed no obvious changes in hypoxic SMMC7721 after HIF-1α knockdown (Fig. 1c). These results indicated that hypoxia-induced upregulation of cZNF292 is not mediated by HIF-1α, and did not significantly correlate with host gene expression.

In order to explore the biological functions of cZNF292 in hypoxic tumor cells, we employed lentiviral-mediated cZNF292 shRNA transfer technique to downregulate cZNF292 expression and generate stable cell lines to analyze phenotypic changes. First, we analyzed cZNF292 expression in hepatoma cells by real-time PCR in order to confirm the knockdown of cZNF292. As shown in Fig. 1d, cZNF292 expression in SMMC7721 cells with cZNF292 shRNA integration was significantly decreased compared with that of control cells, and the knockdown ratio was 84.0%. Then, we examined whether the knockdown of cZNF292 affected its host gene expression because circular transcripts might have cis-regulatory activity on host gene expression [22,26]. We found that ZNF292 mRNA and protein levels showed no significant difference between cZNF292 knockdown group and control group (Fig. 1d,e). The results showed that silencing of cZNF292 did not affect expression of ZNF292, suggesting that a cis-regulatory function of cZNF292 was unlikely.

3.2. cZNF292 knockdown inhibited hepatoma cell proliferation and induced G1 arrest

We investigated the effect of cZNF292 downregulation on normoxic or hypoxic human hepatoma cell viability in vitro by CCK-8 assay. The results showed that cZNF292 knockdown decreased viability of normoxic or hypoxic SMMC7721 cells after 12, 24, 36 and 48 h incubation ($p < .05$ or $p < .01$) (Fig. 2a,b). These results indicated that cZNF292 knockdown significantly suppressed normoxic or hypoxic human hepatoma cell viability in vitro. To investigate the mechanism underlying cZNF292 knockdown mediated cell proliferation suppression, we analyzed cell cycle of human hepatoma cells by flow cytometry after 48 h normoxic or hypoxic culture. It was found that the proportion of G1 phase cells was significantly increased in the knockdown group compared with control group, and the proportion of S phase was significantly decreased ($p < .05$) (Fig. 2c,d). It is well known Wnt/β-catenin signaling is one of the important pathways in cell cycle regulation, and its downstream target molecules c-Myc and CyclinD1 play an important role in G1 to S transition [31,32]. To investigate whether the cZNF292 knockdown-induced G1 arrest was regulated through Wnt/β-catenin signaling pathway, we used western blot to detect the expression changes of Wnt/β-catenin signaling molecules. Our results showed that knockdown of cZNF292 significantly decreased the expression of β-catenin, CyclinD1, and c-Myc protein in hypoxic SMMC7721 cells, and increased the expression of p21 protein (Fig. 2e). The above results indicated that knockdown of cZNF292 might inhibit hepatoma cell proliferation and induce G1 arrest via reducing Wnt/β-catenin signaling pathway activity.

3.3. cZNF292 knockdown did not affect hepatoma cell apoptosis

In order to investigate whether apoptosis was also involved in cZNF292 knockdown-induced decreased viability of SMMC7721 cells, apoptosis of human hepatoma cells were quantitatively measured using flow cytometry after 48 h normoxic or hypoxic culture. The results showed that no obvious change of apoptotic rate was observed between control cells and cZNF292 knockdown cells after normoxic or hypoxic culture (Supplementary Fig. 1). These results indicated that cZNF292 knockdown did not affect hepatoma cell apoptosis.

3.4. cZNF292 knockdown inhibited hepatoma VM by reducing Wnt/β-catenin signaling pathway activity

Previous studies have reported that cZNF292 induced the formation of vascular-like structures in endothelial cells and glioma cells [26,33]. Therefore, we hypothesized that cZNF292 might also have a similar function in hepatoma cells. To verify this conjecture, we studied the effect of cZNF292 knockdown on hepatoma VM formation in matrigel assays. The results showed that under normoxic or hypoxic culture, the number of VM formation of cZNF292 knockdown hepatoma cells was significantly less than that of control cells. We found that vascular-like structure appeared at 3 h after plating, peaked at 6 h, then gradually dissolved and its number decreased in hypoxic or normoxic control group. In addition, the vascular-like structure in hypoxic control group was significantly increased compared with normoxic control group (Fig. 3a,b,c). These results indicated that cZNF292 knockdown inhibited hepatoma VM and hypoxia showed stronger effect than normoxia on inducing hepatoma VM.

It is generally believed that the formation of VM may be related to de-differentiation or trans-differentiation of tumor cells [34]. Vascular endothelial cadherin (VE-cadherin) is a transmembrane adhesion protein expressed between endothelial cells [35]. Under 3-dimensional culture conditions, VE-cadherin can promote the integration of endothelial cells and form a tubular cavity, with the role of induction of angiogenesis [34,36]. Wnt/β-catenin signaling pathway also plays an important role in tumor VM formation. The activation of Wnt/β-catenin signaling pathway up-regulates the expression of β-catenin, activates downstream target genes which directly associated with epithelial-mesenchymal transition (EMT), such as Twist1 and VE-cadherin, and promotes tumor VM formation [36,37]. Based on the above mechanisms, we detected changes in the expression levels of HIF-1α, β-catenin, Twist1, and VE-cadherin in hypoxic SMMC7721 cells after cZNF292 knockdown. cZNF292 knockdown significantly decreased the expression of β-catenin, Twist1 and VE-cadherin protein in hypoxic SMMC7721 cells, while the expression level of HIF-1α protein was not changed significantly (Fig. 3d). The above results indicated that knockdown of cZNF292 may inhibit the formation of hepatoma VM through reducing Wnt/β-catenin signaling pathway activity.

3.5. cZNF292 knockdown enhanced radiosensitivity of SMMC7721 cells by reducing DNA damage repair capacity

After exposure to various dose of X-ray, survival curves of hypoxic and normoxic SMMC7721 cells were obtained. (Fig. 4a,b). The results of clonogenic assay showed that hypoxic SMMC7721 cells with cZNF292 knockdown ($D_0 = 2.75$ Gy) were more sensitive to X-ray irradiation than hypoxic control cells ($D_0 = 3.51$ Gy), and the radiosensitization ratio was 1.28. Under normoxic conditions, SMMC7721 cells with cZNF292 knockdown ($D_0 = 1.56$ Gy) were more sensitive to X-ray irradiation than control cells ($D_0 = 2.02$ Gy), and the radiosensitization ratio was 1.30. The oxygen enhancement ratio (OER) was calculated as the ratio of D_0 (hypoxia) to D_0 (normoxia). The OER value of control cells and cells with cZNF292 knockdown was 1.77 and 1.74, respectively. These results indicated that cZNF292 knockdown could enhance the radiosensitivity of hepatoma cells under hypoxia or normoxic conditions.

To investigate the mechanism of the radiosensitizing effect of cZNF292 knockdown on hepatoma cells, radiation-induced γ-H2AX foci formation was used for examination of DNA damage repair capability of hypoxic and normoxic SMMC7721 cells irradiated by 4 Gy X-ray. The

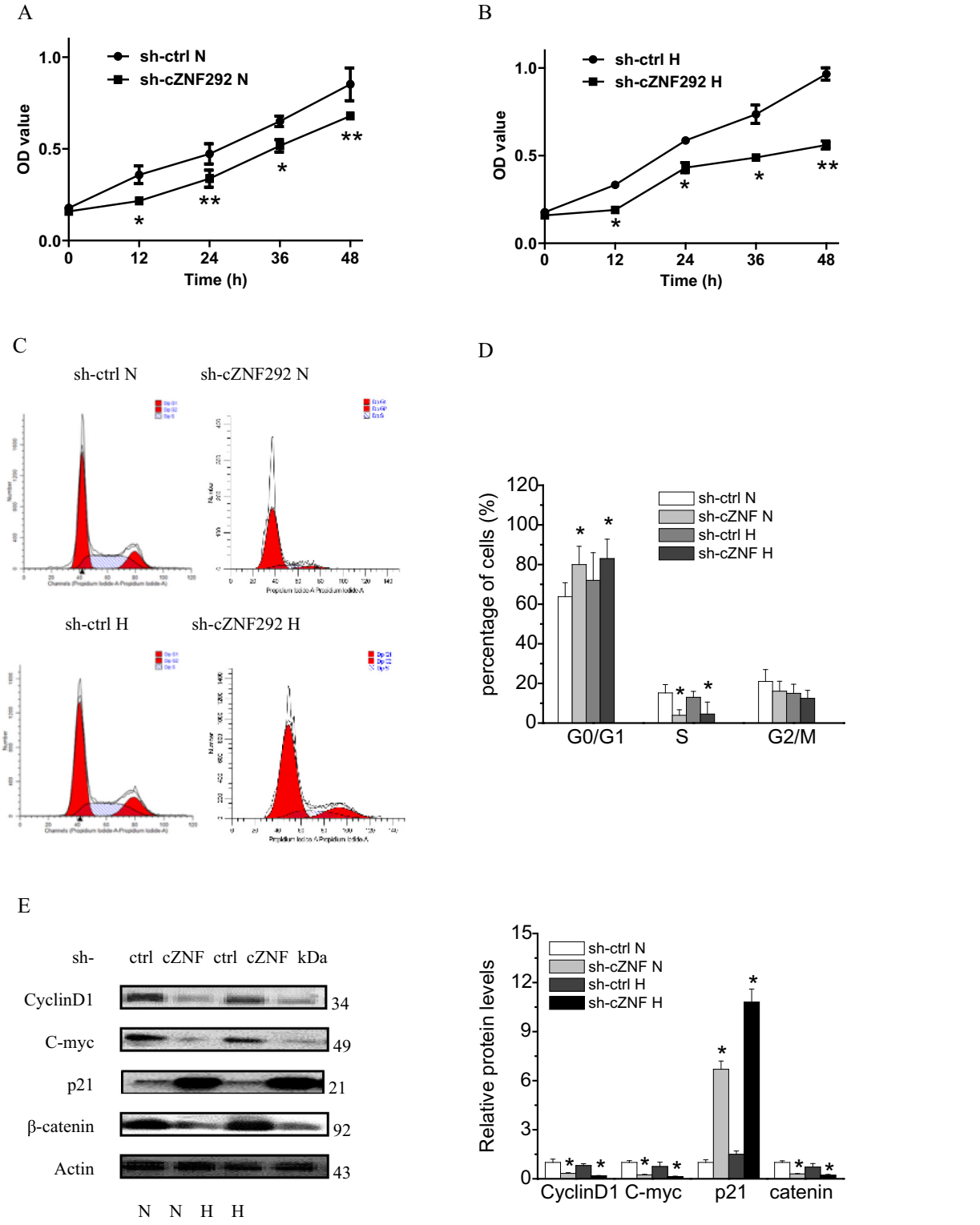

Fig. 2. Effect of cZNF292 knockdown on the proliferation of hypoxic hepatoma cells. a Growth curve of normoxic SMMC7721 cells. b Growth curve of hypoxic SMMC7721 cells. c Cell cycle diagram of normoxic and hypoxic SMMC7721 cells by flow cytometry. d cell cycle distribution of SMMC7721 cells. e The expression changes of Wnt/β-catenin signaling molecules detected by western blot. Data are the means ± SEM of three experiments. *$p < .05$; **$p < .01$.

results showed that the numbers of γ-H2AX foci of cells with cZNF292 knockdown were significantly higher than those of control cells at 0.5, 1, 2, and 4 h after irradiation in both normoxic and hypoxic conditions. The foci number of γH2AX was the highest at 0.5 h after irradiation, then gradually decreased, and go back to the background level at 12 h after irradiation (Fig. 4c,d). Moreover, normoxic cells showed elevated γ-H2AX foci number than hypoxic cells at the same time point. These results indicated that DNA repair capacity of hepatoma cells could be reduced by cZNF292 knockdown, which might be the main reason for its radiosensitizing effect.

It was reported that c-Myc protein participated in the regulation of DNA double-strand break repair and depression of c-Myc resulted in a

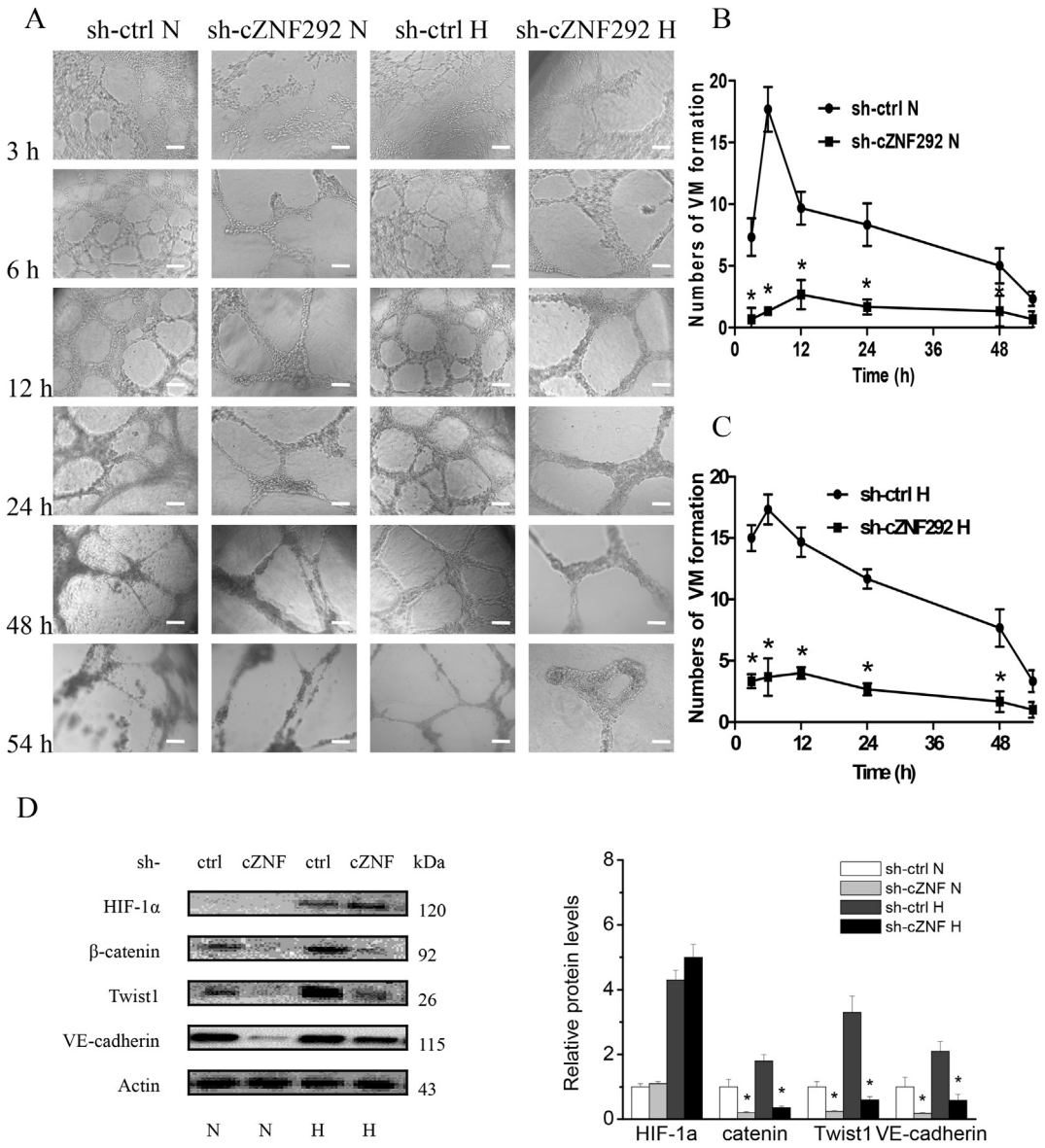

Fig. 3. cZNF292 knockdown inhibited hepatoma VM by reducing Wnt/β-catenin signaling pathway activity. a cZNF292 knockdown on hepatoma tube formation in matrigel assays. Scale bar = 50 μm. b knockdown of cZNF292 on VM of normoxic hepatoma cells at different time points. c knockdown of cZNF292 on VM of hypoxic hepatoma cells at different time points. d VM-related protein expression levels in hypoxic hepatoma cells detected by western blot. Data are the means ± SEM of three experiments. *$p < .01$.

decreased phosphorylation of ataxia telangiectasia mutated (ATM) protein and DNA-dependent protein kinase catalytic subunit (DNA-PKcs) kinase activity and consequently a decreased DSB repair efficiency [38]. As above mentioned, cZNF292 knockdown could down-regulate Wnt/β-catenin pathway downstream target c-Myc expression. Therefore, we hypothesized that cZNF292 knockdown might decrease DNA repair capacity of hepatoma cells through down-regulating the activity of β-catenin/c-Myc/ATM/DNA-PKcs pathway. To verify our hypothesis, western blot was used to detect the phosphorylation levels of ATM (S1981) and DNA-PKcs (S2056) in hypoxic hepatoma cells. It has been reported that the autophosphorylation of DNA-PKcs at S2056 causes DNA-PKcs to separate from Ku, leading to inhibition of DNA-PK catalytic activity [39]. We found the phosphorylation level of DNA-PKcs (S2056) protein was significantly increased in cZNF292 knockdown group, compared with control group, at 0.5 h after irradiation. The phosphorylation level of ATM (S1981) in the control group was significantly increased at 0.5 h after irradiation, while it showed no significant change in cZNF292 knockdown group (Fig. 4e). Moreover, DNA-PKcs kinase activity of hypoxic hepatoma cells with cZNF292 knockdown was significantly decreased, compared with control group, at 0.5 h after irradiation (Fig. 4f). These results indicated that cZNF292 knockdown might result in a decreased phosphorylation of ATM and DNA-PKcs kinase activity, which consequently led to a reduced DSB repair capacity.

3.6. cZNF292 inhibits SOX9 protein nuclear translocation by binding it and consequently activates the Wnt/β-catenin pathway

The above results showed that cZNF292 could regulate Wnt/β-catenin signaling pathway, but its molecular mechanisms remained to be studied. We used RNA-binding protein immunoprecipitation (RIP) assays to detect Wnt/β-catenin pathway-associated proteins that may interact with cZNF292, including β-catenin, adenomatous polyposis coli (APC), axis inhibition (Axin), SOX protein repression of Wnt/β-catenin signaling: SOX6, SOX9 and SOX17, and HIF-1α, in hypoxia. Real-Time PCR detection of cZNF292 and linear ZNF292 mRNA levels

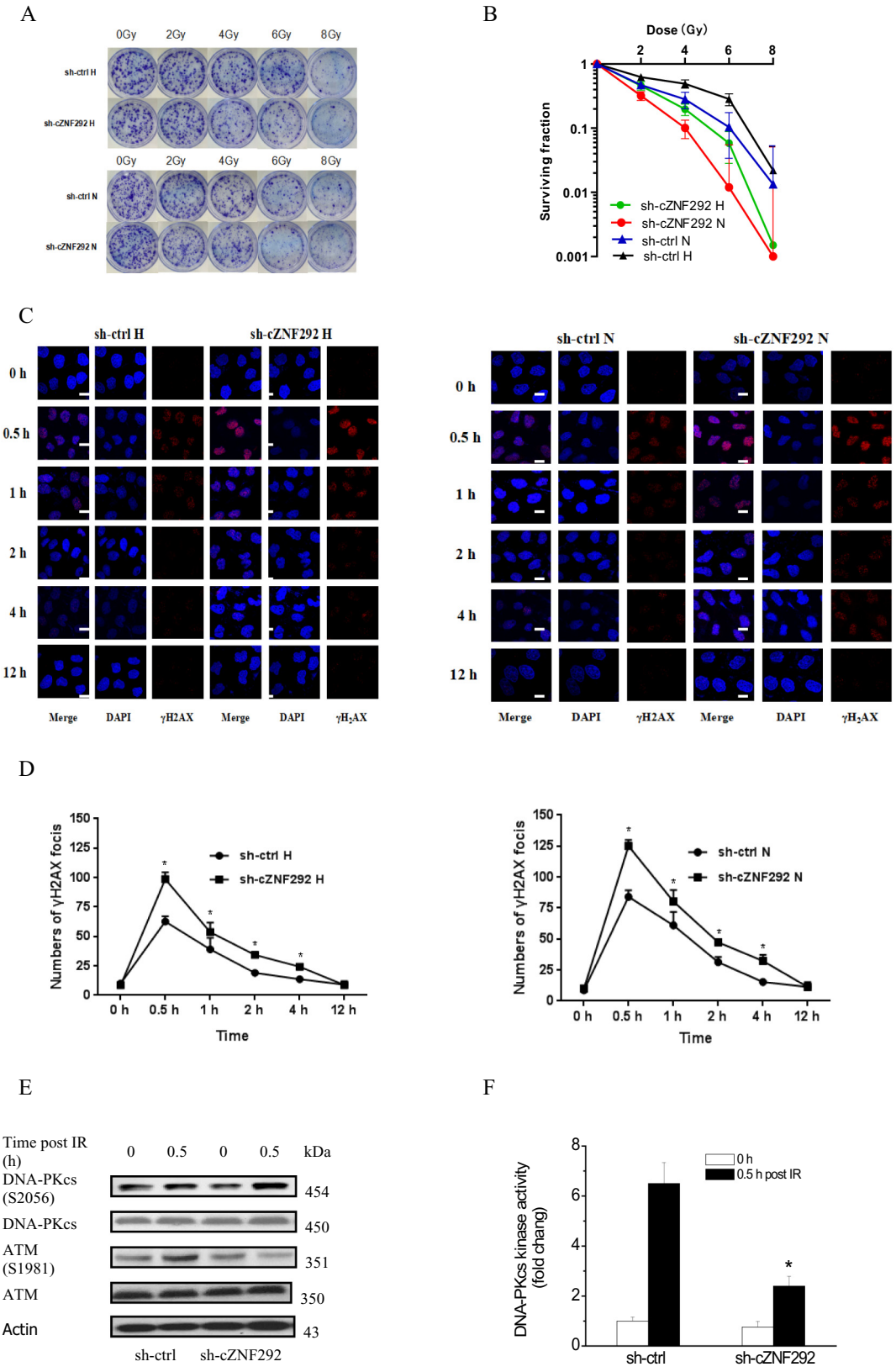

Fig. 4. Effect of cZNF292 knockdown on radiosensitivity and DNA damage repair of hepatocellular carcinoma cells. a Crystal violet staining for colony formation of hypoxic and normoxia SMMC7721 cells after irradiation. b Survival curves of hypoxic and normoxic SMMC7721 cells. c Radiation-induced γ-H2AX foci formation in SMMC7721 cells. Scale bar = 5 μm. d Radiation-induced γ-H2AX foci formation curves of hypoxic and normoxic SMMC7721 cells. e phosphorylation levels of ATM (S1981) and DNA-PKcs (S2056) in hypoxic hepatoma cells detected by western blot. Data are the means ± SEM of three experiments. *$p < .05$. f DNA-PKcs kinase activity was measured in hypoxic hepatoma cells. Data are the means ± SEM of three experiments. *$p < .01$. (For interpretation of the references to colour in this figure legend, the reader is referred to the web version of this article.)

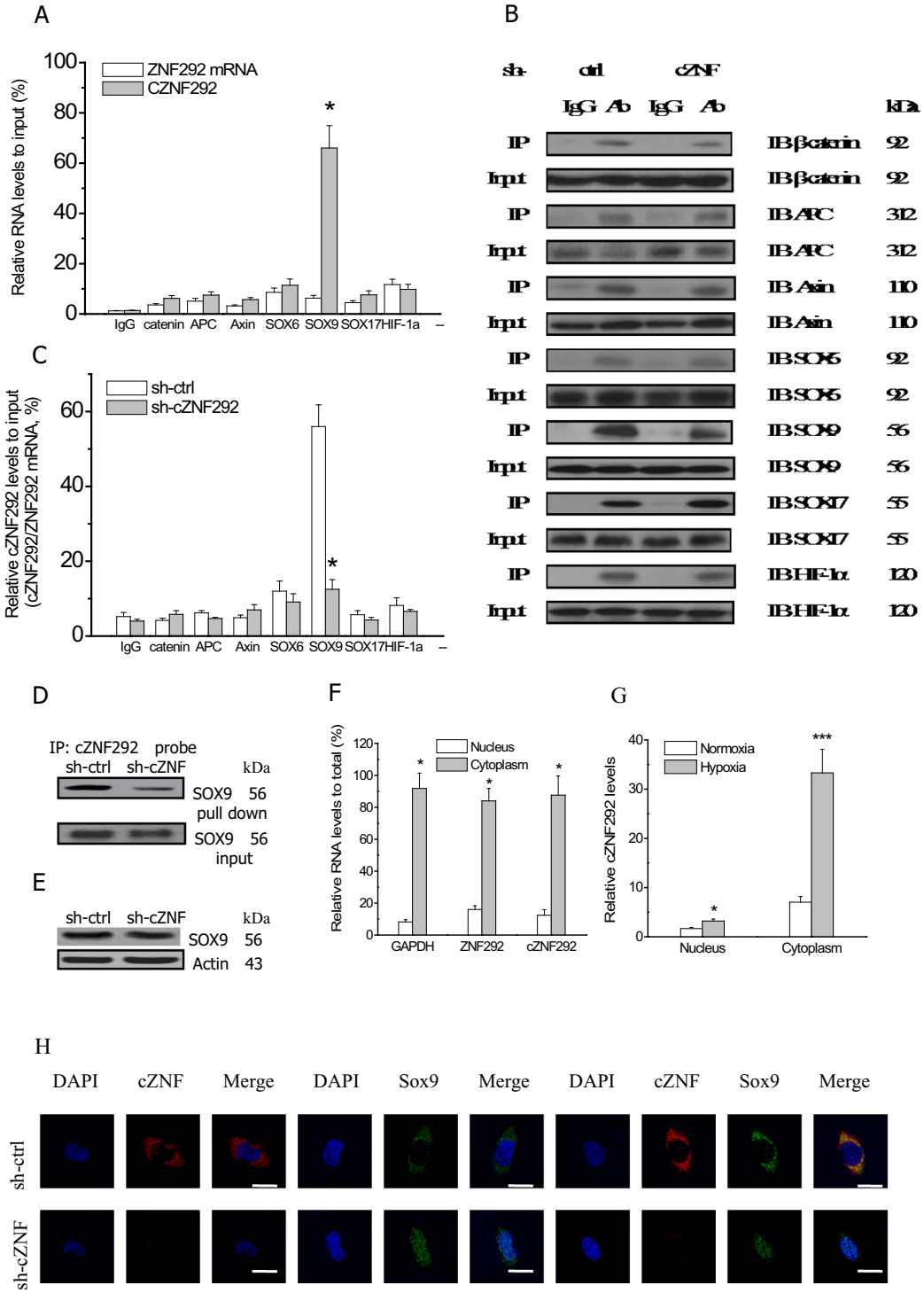

Fig. 5. cZNF292 inhibits SOX9 protein nuclear translocation by binding it and consequently activates the Wnt/β-catenin pathway. a cZNF292 was pulled-down only by SOX9 antibody (*$p < .001$). b Western blot results showed that immunoprecipitation pulled down similar amount of proteins between control and cZNF292 knockdown cells. c cZNF292 levels pulled-down by SOX9 antibody decreased significantly after cZNF292 knockdown (*$p < .001$). d The biotinylated probe designed to specifically detect cZNF292 pulled down decreased levels of SOX9 protein after cZNF292 knockdown. e Knockdown of cZNF292 did not affect SOX9 protein expression in hypoxic hepatoma cells. f cZNF292, GADPH and ZNF292 were mainly expressed in the cytoplasm (*$p < .001$). g Hypoxia-induced cZNF292 expression was mainly distributed in the cytoplasm (*$p < .05$; ***$p < .001$). h Confocal laser scanning microscopy observation of the effect of cZNF292 on the localization of most SOX9 to the cytoplasm. Scale bar = 5 μm. Data are the means ± SEM of three experiments.

using specific primers revealed that cZNF292 was pulled-down only by SOX9 antibody, and linear ZNF292 mRNA was not pulled-down by SOX9 antibody (Fig. 5a). Further, we used hypoxic hepatoma cell lysates of cZNF292 knockdown group and control group to immunoprecipitate with the above antibodies, and detected cZNF292 levels using Real-Time PCR. The western blot results showed that immunoprecipitation pulled down similar amount of proteins in both control and cZNF292 knockdown cells (Fig. 5b). Then, the

immunoprecipitated mixtures were subject to Real-Time PCR with primers specific for cZNF292. The results showed that cZNF292 levels pulled-down by SOX9 antibody were decreased significantly in cZNF292 knockdown group, compared with control group, and cZNF292 levels pulled-down by other antibodies showed no significant changes between cZNF292 knockdown group and control group (Fig. 5c). In addition, Lysates from hypoxic cZNF292 knockdown cells or control cells were incubated with a biotinylated probe designed to specifically detect cZNF292. The mixture was incubated with streptavidin beads followed by western blot analysis. The results showed that the probe pulled down decreased levels of SOX9 protein in hypoxic cZNF292 knockdown cells than control cells (Fig. 5d). In order to determine whether cZNF292 knockdown affected SOX9 protein expression or not, we detected the SOX9 protein levels in hypoxic knockdown and control cells by Western blot. It was found that knockdown of cZNF292 did not affect SOX9 protein expression in hypoxic hepatoma cells (Fig. 5e). These results indicated that cZNF292 might interact with SOX9 protein in hepatoma cells.

To locate cZNF292 distribution in cells, we extracted the cytoplasmic and nuclei RNA of SMMC7721 cells. Real-time PCR detection of cZNF292 and linear ZNF292 mRNA levels revealed that cZNF292, GADPH and ZNF292 were mainly localized in the cytoplasm (Fig. 5f). Further, we found that hypoxia-induced cZNF292 was mainly distributed in the cytoplasm (Fig. 5g). Hypoxic cZNF292 knockdown cells and control cells were also subject to in situ hybridization. In confocal laser scanning microscopy observation, SOX9 protein was detected in the cytoplasm and nucleus, whereas cZNF292 knockdown facilitated nuclear translocation of SOX9, suggesting the effect of cZNF292 on the localization of most SOX9 to the cytoplasm (Fig. 5h). This was consistent with the distribution of cZNF292 in the cytoplasm. SOX9 could interact directly with β-catenin and antagonise its activity by competing with β-catenin for its partner T-cell factor/lymphoid enhancer factor (TCF/LEF) and promoting its degradation via the ubiquitin proteasome pathway [40,41]. The above results suggested that hypoxia might induce cZNF292 expression, which binded to SOX9 protein in cytoplasm and inhibited its nuclear translocation, resulting in enhanced Wnt/β-catenin pathway activity. Conversely, knockdown of cZNF292 will increase SOX9 nuclear translocation, subsequently reduce Wnt/β-catenin pathway activity, leading to inhibition of hypoxic hepatoma cell proliferation, VM, and radioresistance.

3.7. β-catenin overexpression or SOX9 knockdown rescued radioresistance of hypoxic SMMC7721 cells with cZNF292 knockdown

To identify whether the reduced radioresistance of hypoxic SMMC7721 cells caused by cZNF292 knockdown could be recovered by β-catenin overexpression or SOX9 knockdown, overexpression recombinant vector pcDNA-β-catenin and SOX9-siRNA were used to block the effect of cZNF292 knockdown. As shown in Fig. 6a, protein expression of Wnt/β-catenin pathway downstream target c-Myc significantly increased in sh-cZNF292 + pcDNA-β-catenin or sh-cZNF292 + SOX9-siRNA comparing to sh-cZNF292 + pcDNA3.1 or sh-cZNF292 + nc-siRNA after 48 h hypoxic incubation, respectively. In addition, We found the phosphorylation level of DNA-PKcs (S2056) protein was significantly decreased and the phosphorylation level of ATM (S1981) was significantly increased in hypoxic sh-cZNF292 + pcDNA-β-catenin or sh-cZNF292 + SOX9-siRNA comparing to hypoxic sh-cZNF292 + pcDNA3.1 or sh-cZNF292 + nc-siRNA, at 0.5 h after irradiation, respectively (Fig. 6b). To investigate whether β-catenin overexpression or SOX9 knockdown could rescue radioresistance of hypoxic SMMC7721 cells with cZNF292 knockdown, we examined radiosensitivity by clonogenic assay 48 h after β-catenin expression vectors or SOX9-siRNA transfection. The results showed that hypoxic SMMC7721 cells with β-catenin overexpression (D_0 = 3.22 Gy) or SOX9 knockdown (D_0 = 3.30 Gy) were more resistant to X-ray irradiation than SMMC7721 cells with cZNF292 knockdown (D_0 = 2.73 Gy) (Fig. 6c). These results indicated that β-catenin overexpression or SOX9 knockdown could rescue radioresistance of hypoxic SMMC7721 cells with cZNF292 knockdown, validating the above mentioned molecular mechanisms about the radiosensitizing effect of cZNF292 knockdown on hypoxic SMMC7721 cells.

3.8. Effect of cZNF292 knockdown in combination with radiotherapy on human hepatoma xenograft growth and survival of athymic nude mice

The tumors were irradiated with 8 Gy (2 Gy/d for 4 successive days) after dividing, followed by detection of hepatoma xenograft growth (Fig. 7a). It can be seen that the tumor volume was significantly decreased in mice of radiotherapy group (from day 6 to 21, $p < .001$), cZNF292 knockdown group (from day 6 to 21, $p < .01$ or $p < .001$) and combined therapy group (from day 6 to 21, $p < .001$) compared with control group. The tumor volume in mice of negative control vector group showed no significant change compared with control group (from day 3 to 21, $p > .05$). The average tumor volume reached 1268 mm^3 in mice of control group on day 21, while only 417 mm^3 (32.89% of control) in combined therapy group, 907 mm^3 (71.53% of control) in cZNF292 knockdown group, and 684 mm^3 (53.94% of control) in radiotherapy group. In addition, the tumor volume was significantly decreased in mice of combined therapy group compared with cZNF292 knockdown (from day 9 to 21, $p < .01$ or $p < .001$) or radiotherapy group (from day 12 to 21, $p < .01$ or $p < .001$).

The long-term outcome of cZNF292 knockdown in combination with radiotherapy was evaluated by survival rates of mice subcutaneously implanted human hepatoma. Results of survival were evaluated using Kaplan-Meier (Fig. 7b). The median survival of control, negative control vector, radiotherapy, cZNF292 knockdown and combined therapy group was 45.33 ± 5.75, 44.67 ± 7.81, 72.83 ± 6.34, 55.0 ± 8.67 and 86.0 ± 6.20 days, respectively. Survival durations were significantly longer in radiotherapy group ($p < .001$), cZNF292 knockdown group ($p < .001$) and combined therapy group ($p < .001$) compared with control group. Survival durations were significantly longer in combined therapy group compared with radiotherapy ($p < .001$) or cZNF292 knockdown group ($p < .001$).

3.9. Effect of cZNF292 knockdown in combination with radiotherapy on cell proliferation, apoptosis, tumor angiogenesis and VM formation in human hepatoma xenograft

First, effect of cZNF292 knockdown in combination with radiotherapy on cell proliferation in human hepatoma xenograft was examined by Ki-67 staining, which is a specific marker of proliferating cell. In microscopic observation of tumors, lesser number of Ki-67-positive cells was observed in cZNF292 knockdown group ($p < .01$), 8 Gy group ($p < .05$) and combined therapy group ($p < .01$) compared with control group as shown in Fig. 8a. Ki-67-positive cells was significantly decreased in combined therapy group compared with 8 Gy group ($p < .01$) or cZNF292 knockdown group ($p < .01$).

Next, we investigated the effect of cZNF292 knockdown in combination with radiotherapy on tumor angiogenesis and VM formation in human hepatoma xenograft by CD31- periodic acid solution (PAS) double staining. Different from the traditional endothelial-dependent vessels, vasculogenic mimicry is absent of endothelial cells in the inner wall of the pipe, and directly surrounded by tumor cells [30]. CD31 is a marker of endothelial cells, and the basement membrane is positive for PAS [42]. Therefore, we counted PAS-positive and CD31-positive as endothelial-dependent vessels and PAS-positive and CD31-negative vessels as VM.

The microscopic examination revealed lower tumor microvessel density (MVD) in treatment groups of tumors as shown in Fig. 8b. The quantification of tumor microvessel density showed 8.51 ± 2.07, 5.22 ± 1.00, 4.09 ± 1.60 and 2.78 ± 0.35 in control, cZNF292 knockdown, 8 Gy and combined therapy group, respectively. MVD was

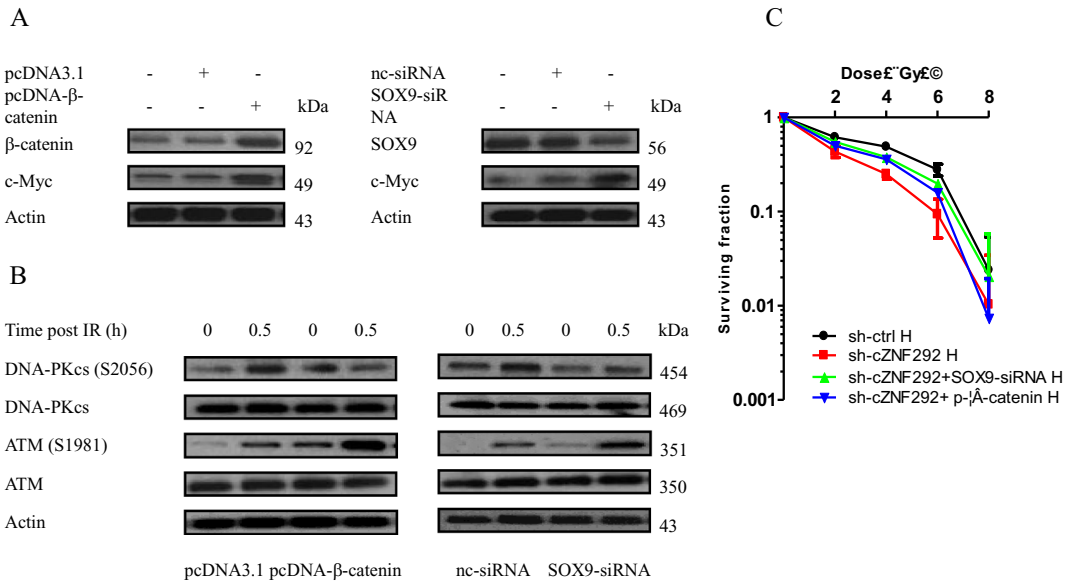

Fig. 6. β-catenin overexpression or SOX9 knockdown rescued radioresistance of hypoxic SMMC7721 cells with cZNF292 knockdown. a β-catenin overexpression or SOX9 knockdown rescued protein expression of Wnt/β-catenin pathway downstream target c-Myc. b. β-catenin overexpression or SOX9 knockdown decreased the phosphorylation level of DNA-PKcs (S2056) protein, and increased the phosphorylation level of ATM (S1981) protein. c β-catenin overexpression or SOX9 knockdown rescued radioresistance of hypoxic SMMC7721 cells with cZNF292 knockdown. Data are the means ± SEM of three experiments.

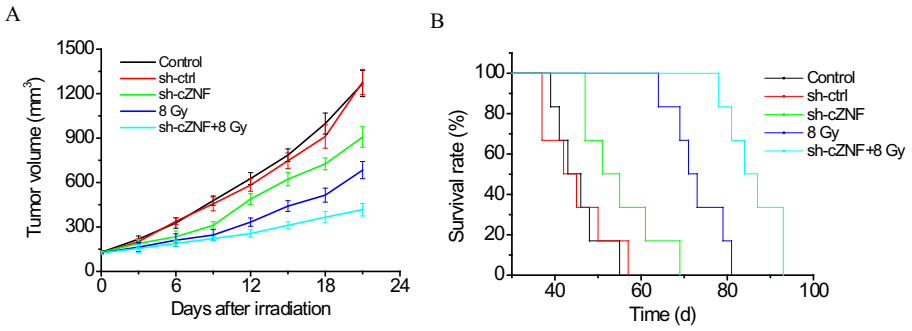

Fig. 7. Effect of cZNF292 knockdown in combination with radiotherapy on human hepatoma xenograft growth and survival of athymic nude mice. a Detection of hepatoma xenograft growth. b Results of survival were evaluated using Kaplan-Meier.

significantly decreased in combined therapy group compared with 8 Gy group ($p < .01$) or cZNF292 knockdown group ($p < .01$).

Microscopic examination of vasculogenic mimicry density (VMD) showed an decrease in cZNF292 knockdown and combined therapy group compared with control group as shown in Fig. 8b. VMD of 8 Gy group showed no significant changes compared with control group.

TUNEL staining was performed to assess the apoptotic effect of cZNF292 knockdown in combination with radiotherapy in tumors, which showed an increased number of TUNEL-positive cells in 8 Gy and combined therapy group compared with control group as shown in Fig. 8c. The quantification of TUNEL staining showed 4.60 ± 1.42%, 5.20 ± 1.23%, 11.89 ± 2.58% and 28.47 ± 4.88% positive cells in control, cZNF292 knockdown, 8 Gy and combined therapy group, respectively. TUNEL-positive cells was significantly increased in combined therapy group compared with 8 Gy group ($p < .01$).

4. Discussion

Hypoxia is a classic feature of the tumor microenvironment with a profound impact on cancer progression and therapeutic response. During the process of tumor development, cancer cells inside a solid tumor can suffer from three major types of hypoxia, chronic diffusion hypoxia, acute/intermittent perfusion hypoxia, or/and anemic hypoxia, owing to the abnormal growth of tumor vasculature, increased tumor size, and reduced oxygen concentration in the blood [43].

Well-oxygenated cells respond better to radiotherapy by a factor 2.5–3, compared to cells in anoxic regions [44]. The ratio of hypoxic to aerated doses needed to achieve the same biological effect is called the oxygen enhancement ratio (OER). The mechanism of the oxygen effect is most commonly explained by the oxygen fixation hypothesis, mainly on the chemical level, which postulates that radical-induced DNA damage can be permanently 'fixed' by molecular oxygen, rendering DNA damage irreparable [45]. At the cellular and molecular biology level, the mechanism of radioresistance of hypoxic tumor cells needs to be further explained, and has been one of the focuses of radiation oncology and radiobiology research.

A growing number of studies have shown that tumor hypoxia induces multiple gene transcription, non-coding RNA and protein expression, directly or indirectly affecting tumor radiation sensitivity [46–48]. Signaling transduction of hypoxia pathways orchestrated by the transcription factor HIF contributes to aggressive phenotypes and metastasis in numerous cancers [49,50]. Hypoxia has been clearly established as a key epigenetic factor modulating the outcome of radiotherapy. Over the past few decades, continually increasing research indicated the importance of the non-coding RNA in tumor hypoxic microenvironment. Circular RNAs (circRNAs) are a recently discovered

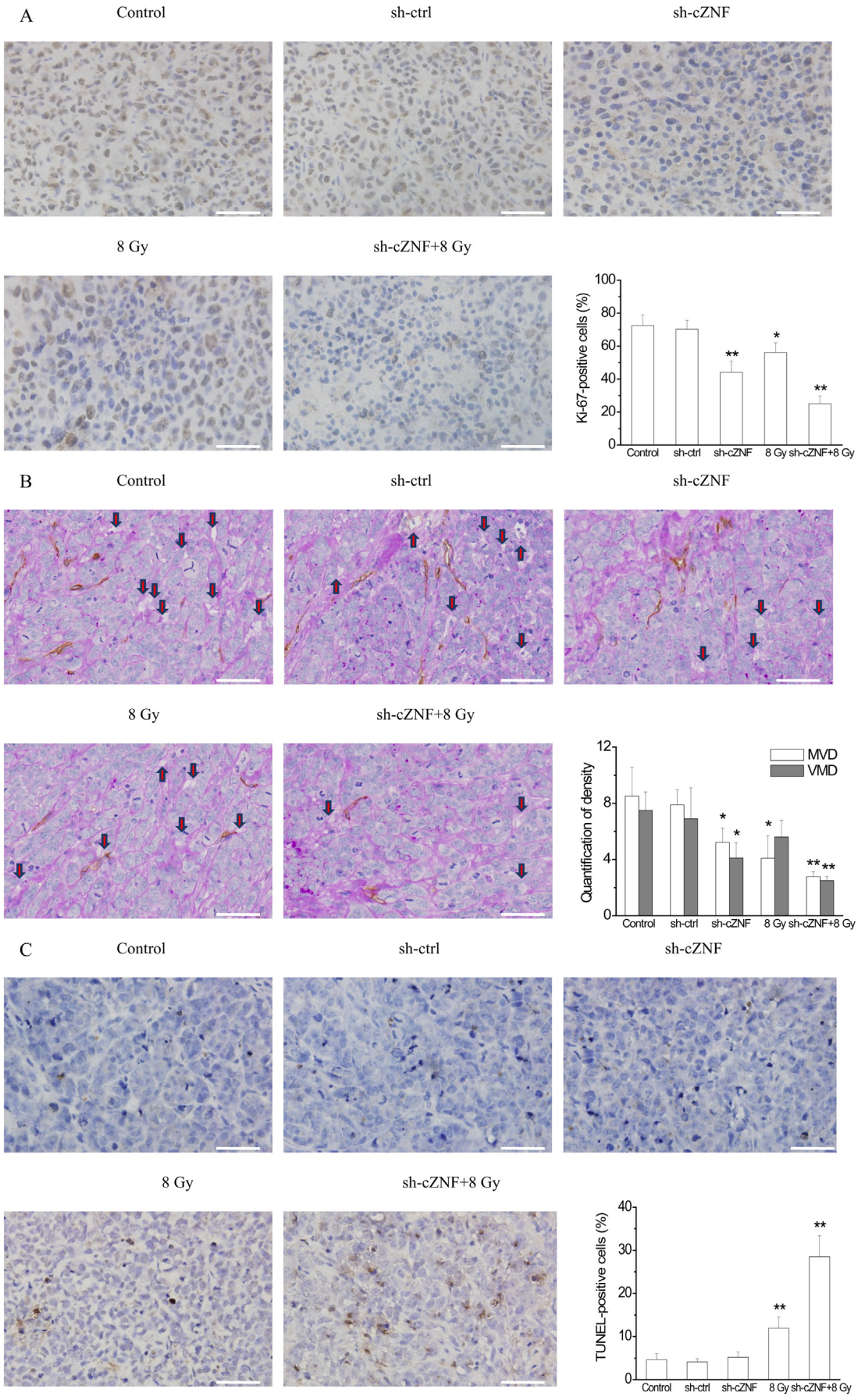

(caption on next page)

Fig. 8. Effect of cZNF292 knockdown in combination with radiotherapy on cell proliferation, apoptosis, tumor angiogenesis and VM formation in human hepatoma xenograft. a Effect of cZNF292 knockdown in combination with radiotherapy on cell proliferation in human hepatoma xenograft was examined by Ki-67 staining. b Effect of cZNF292 knockdown in combination with radiotherapy on tumor angiogenesis and VM formation in human hepatoma xenograft were examined by CD31-PAS double staining. Arrow: structure of VM. c TUNEL staining was performed to assess the apoptotic effect of cZNF292 knockdown in combination with radiotherapy in tumors. Scale bar = 100 μm. Data are the means ± SEM of three experiments. *$p < .05$; **$p < .01$.

non-coding RNAs, which have been shown to be involved in multiple physiological and pathological processes [19–21]. Moreover, circRNAs can not only be found in different tissues, organs but also enriched in body fluids, such as blood, exosomes, saliva, seminal plasma, suggesting that circRNAs might be promising biomarkers and therapy targets for human disease [51–53]. So far, it is regarded that circRNAs can function in multiple biological processes, such as miRNA binding, protein binding and regulation of transcription and post-transcription [54].

cZNF292 is a circRNA that regulates the biological function of both endothelial cells and tumor cells [26,33]. Boeckel et al. first identified endothelial circRNAs by computational analysis of ribo-minus RNA generated from human umbilical venous endothelial cells cultured under normoxic or hypoxic conditions. They found that the majority of them lacks polyadenylation, is resistant to RNase R digestion and localized to the cytoplasm, and further validated the hypoxia-induced circRNAs, including cZNF292, by RT-PCR. Cloning of cZNF292 validated the predicted back splicing of exon 4 to a new alternative exon 1A. Silencing of cZNF292 reduced tube formation and spheroid sprouting of endothelial cells in vitro. Moreover, They revealed that cZNF292 had no validated microRNA-binding sites detected in argonaute high-throughput sequencing of RNA isolated by cross-linking and immunoprecipitation data sets, suggesting that cZNF292 does not act as a microRNA sponge [26]. A recent study revealed that cZNF292 played an important role in glioma proliferation and tube formation, the mechanism of which may involve the regulation of cell cycle [33]. However, more in-depth mechanistic studies are needed to further understand the mechanism of cZNF292 function. In this study, we found that cZNF292 could be induced by hypoxia in a time-dependent manner in hepatoma cells independent of hypoxia inducible factor (HIF)-1α and host gene expression. It has been demonstrated that hypoxia regulated kinases that interfered with splicing and modulated the expression and activity of JmjC domain-containing proteins, which interacted with splicing factors [55,56], so hypoxia might induce generation of circRNAs through regulating back-splicing. The mechanism by which ZNF292 circularization is induced by hypoxia deserves further exploration. Moreover, we found knockdown of cZNF292 increased SOX9 nuclear translocation, subsequently reduced Wnt/β-catenin pathway activity, leading to suppression of hypoxic hepatoma cell proliferation, VM, and radioresistance in vitro. SOX9 is a member of the E subfamily of the SOX gene family. It is a nuclear transcription factor and plays an important role in tumorigenesis, development, and metastasis [40]. SOX9 regulates negatively the activity of Wnt/β-catenin pathway through competing with β-catenin to bind TCF/LEF (TCF/LEF), enhancing β-catenin phosphorylation and promoting its degradation [40,41]. Here, we show cZNF292 could co-localize and bind with SOX9 protein in the cytoplasm. Similarly, it has been reported that circFoxo3, which was downregulated in cancer cells and was associated with cell cycle progression, also interacted with some proteins in the cytoplasm [28,29]. We subcutaneously implanted human hepatoma SMMC7721 cells in the right hind legs of athymic nude mice to explore the anti-cancer effect of cZNF292 knockdown in combination with radiotherapy in vivo. Results showed that cZNF292 knockdown in combination with radiotherapy were more effective than radiotherapy alone or cZNF292 knockdown alone in suppressing tumor growth and extending survival duration. Analysing associated mechanisms of the in vivo efficacy of combination therapy, we observed its moderate inhibitory effects on cell proliferation and tumor angiogenesis and VM, as well as a strong enhancing effect on apoptosis in tumor xenograft.

In summary, our studies uncovered a novel mechanism of cZNF292 in enhancing hypoxic human hepatoma SMMC7721 cell radiosensitivity, which laid a theoretical and experimental foundation for the application of circRNAs as radiosensitizing agent for cancer radiotherapy.

Acknowledgements

The work was supported by National Natural Science Foundation of China (31570851, 31870844 and 81874080), A Project Funded by the Priority Academic Program Development of Jiangsu Higher Education Institutions (PAPD) and Study Abroad Scholarship of Jiangsu Provincial Government.

Conflict of interest

The authors declare that they have no conflict of interest.

Appendix A. Supplementary data

Supplementary data to this article can be found online at https://doi.org/10.1016/j.cellsig.2019.04.011.

References

[1] K.A. Mcglynn, J.L. Petrick, W.T. London, Global epidemiology of hepatocellular carcinoma: an emphasis on demographic and regional variability, Clinics in Liver Disease 19 (2015) 223–238.
[2] Global Burden of Disease Liver Cancer Collaboration, et al., The burden of primary liver Cancer and underlying etiologies from 1990 to 2015 at the global, regional, and National Level: results from the global burden of disease study 2015, JAMA Oncology 3 (2017) 1683–1691.
[3] K. Okushin, et al., *Helicobacter pylori* infection and liver diseases: epidemiology and insights into pathogenesis, World Journal of Gastroenterology 24 (2018) 3617–3625.
[4] J.K. DiStefano, Long noncoding RNAs in the initiation, progression, and metastasis of hepatocellular carcinoma, Noncoding RNA Res. 2 (2017) 129–136.
[5] M.C. Pavel, J. Fuster, Expansion of the hepatocellular carcinoma Milan criteria in liver transplantation: future directions, World Journal of Gastroenterology 24 (2018) 3626–3636.
[6] W.Y. Lau, E.C. Lai, Hepatocellular carcinoma. Current management and recent advances, Hepatobiliary & Pancreatic Diseases International 7 (2008) 237–257.
[7] A.L. Harris, Hypoxia–a key regulatory factor in tumour growth, Nature Reviews. Cancer 2 (2002) 38–47.
[8] L. Wilde, et al., Metabolic coupling and the reverse Warburg effect in cancer: implications for novel biomarker and anticancer agent development, Seminars in Oncology 44 (2017) 198–203.
[9] G.L. Semenza, Targeting HIF-1 for cancer therapy, Nature Reviews. Cancer 3 (2003) 721–732.
[10] A. Laitala, J.T. Erler, Hypoxic Signalling in tumour stroma, Frontiers in Oncology 8 (2018) 189.
[11] H. Choudhry, A.L. Harris, Advances in hypoxia-inducible factor biology, Cell Metabolism 27 (2018) 281–298.
[12] D.R. Grimes, D.R. Warren, S. Warren, Hypoxia imaging and radiotherapy: bridging the resolution gap, The British Journal of Radiology 90 (2017) 20160939.
[13] M.R. Horsman, L.S. Mortensen, J.B. Petersen, M. Busk, J. Overgaard, Imaging hypoxia to improve radiotherapy outcome, Nature Reviews. Clinical Oncology 9 (2012) 674–687.
[14] S. Rey, L. Schito, M. Koritzinsky, B.G. Wouters, Molecular targeting of hypoxia in radiotherapy, Advanced Drug Delivery Reviews 109 (2017) 45–62.
[15] Z. Sun, et al., Emerging role of exosome-derived long non-coding RNAs in tumor microenvironment, Molecular Cancer 17 (2018) 82.
[16] H. Liu, et al., Nuclear functions of mammalian MicroRNAs in gene regulation, immunity and cancer, Molecular Cancer 17 (2018) 64.
[17] J. Hou, et al., Circular RNAs and exosomes in cancer: a mysterious connection, Clin. Transl.Oncol. 20 (2018) 1109–1116.
[18] Z. Xin, Q. Ma, S. Ren, G. Wang, F. Li, The understanding of circular RNAs as special triggers in carcinogenesis, Briefings in Functional Genomics 16 (2017) 80–86.
[19] J. Li, et al., Circular RNAs in cancer: novel insights into origins, properties, functions and implications, American Journal of Cancer Research 5 (2015) 472–480.

[20] S.J. Conn, et al., The RNA binding protein quaking regulates formation of circRNAs, Cell 160 (2015) 1125–1134.
[21] X. Cui, et al., Emerging function and potential diagnostic value of circular RNAs in cancer, Molecular Cancer 17 (1) (2018) 123.
[22] S. Memczak, et al., Circular RNAs are a large class of animal RNAs with regulatory potency, Nature 495 (2013) 333–338.
[23] F. Wang, A.J. Nazarali, S. Ji, Circular RNAs as potential biomarkers for cancer diagnosis and therapy, American Journal of Cancer Research 6 (2016) 1167–1176.
[24] J. He, Q. Xie, H. Xu, J. Li, Y. Li, Circular RNAs and cancer, Cancer Letters 396 (2017) 138–144.
[25] L.S. Kristensen, T.B. Hansen, M.T. Venø, J. Kjems, Circular RNAs in cancer: opportunities and challenges in the field, Oncogene 37 (2018) 555–565.
[26] J.N. Boeckel, et al., Identification and characterization of hypoxia-regulated endothelial circular RNA, Circulation Res 117 (2015) 884–890.
[27] W. Yang, Y. Liu, R. Gao, H. Yu, T. Sun, HDAC6 inhibition induces glioma stem cells differentiation and enhances cellular radiation sensitivity through the SHH/Gli1 signaling pathway, Cancer Letters 415 (2018) 164–176.
[28] W.W. Du, et al., Foxo3 circular RNA promotes cardiac senescence by modulating multiple factors associated with stress and senescence responses, European Heart Journal 38 (2017) 1402–1412.
[29] W.W. Du, et al., Foxo3 circular RNA retards cell cycle progression via forming ternary complexes with p21 and CDK2, Nucleic Acids Research 44 (2016) 2846–2858.
[30] Z.J. Liu, et al., In vitro and in vivo apatinib inhibits vasculogenic mimicry in melanoma MUM2B cells, PLoS One 13 (2018) e0200845.
[31] M. Trautmann, et al., SS18-SSX fusion protein-induced Wnt/β-catenin signaling is a therapeutic target in synovial sarcoma, Oncogene 33 (2014) 5006–5016.
[32] J. Mao, et al., UBR2 enriched in p53 deficient mouse bone marrow mesenchymal stem cell-exosome promoted gastric Cancer progression via Wnt/β-catenin pathway, Stem Cells 35 (2017) 2267–2279.
[33] P. Yang, et al., Silencing of cZNF292 circular RNA suppresses human glioma tube formation via the Wnt/β-catenin signaling pathway, Oncotarget 7 (2016) 63449–63455.
[34] K. Liu, et al., Hypoxia induced epithelial-mesenchymal transition and vasculogenic mimicry formation by promoting Bcl-2/Twist1 cooperation, Experimental and Molecular Pathology 99 (2015) 383–391.
[35] B. Georg, G. Marianne, R. Maryam, Endothelial cadherins in cancer, Cell and Tissue Research 355 (2014) 523–527.
[36] L. Qi, et al., Wnt3a promotes the Vasculogenic mimicry formation of Colon Cancer via Wnt/β-catenin signaling, International Journal of Molecular Sciences 16 (2015) 18564–18579.
[37] L. Qi, et al., Wnt3a expression is associated with epithelial-mesenchymal transition and promotes colon cancer progression, Journal of Experimental & Clinical Cancer Research 33 (2014) 107.
[38] F. Cui, et al., The involvement of c-Myc in the DNA double-strand break repair via regulating radiation-induced phosphorylation of ATM and DNA-PKcs activity, Molecular and Cellular Biochemistry 406 (1–2) (2015) 43–51.
[39] D.W. Chan, S.P. Lees-Miller, The DNA-dependent protein kinase is inactivated by autophosphorylation of the catalytic subunit, The Journal of Biological Chemistry 271 (1996) 8936–8941.
[40] H. Akiyama, et al., Interactions between Sox9 and beta-catenin control chondrocyte differentiation, Genes & Development 18 (2004) 1072–1087.
[41] P. Bernard, V.R. Harley, Acquisition of SOX transcription factor specificity through protein-protein interaction, modulation of Wnt signalling and post-translational modification, The International Journal of Biochemistry & Cell Biology 42 (2010) 400–410.
[42] J. Lin, et al., Long non-coding RNA UBE2CP3 enhances HCC cell secretion of VEGFA and promotes angiogenesis by activating ERK1/2/HIF-1α/VEGFA signalling in hepatocellular carcinoma, Journal of Experimental & Clinical Cancer Research 37 (2018) 113.
[43] X.X. Xiong, X.Y. Qiu, D.X. Hu, X.Q. Chen, Advances in hypoxia-mediated mechanisms in hepatocellular carcinoma, Molecular Pharmacology 92 (2017) 246–255.
[44] D. Ewing, The oxygen fixation hypothesis: a reevaluation, American Journal of Clinical Oncology 21 (1998) 355–361.
[45] D.R. Grimes, M. Partridge, A mechanistic investigation of the oxygen fixation hypothesis and oxygen enhancement ratio, Biomed. Phys. Eng. Express 1 (2015) 045209.
[46] I.N. Mistry, M. Thomas, E.D. Calder, S.J. Conway, E.M. Hammond, Clinical advances of hypoxia-activated prodrugs in combination with radiation therapy, International Journal of Radiation Oncology, Biology, Physics 98 (2017) 1183–1196.
[47] H. Harada, How can we overcome tumor hypoxia in radiation therapy? Journal of Radiation Research 52 (2011) 545–556.
[48] W. Yang, et al., Downregulation of miR-210 expression inhibits proliferation, induces apoptosis and enhances radiosensitivity in hypoxic human hepatoma cells in vitro, Experimental Cell Research 318 (2012) 944–954.
[49] C. Liu, Q. Lin, Z. Yun, Cellular and molecular mechanisms underlying oxygen-dependent radiosensitivity, Radiation Research 183 (2015) 487–496.
[50] E.B. Rankin, A.J. Giaccia, Hypoxic control of metastasis, Science 352 (2016) 175–180.
[51] J.H. Bahn, et al., The landscape of microRNA, Piwi-interacting RNA, and circular RNA in human saliva, Clinical Chemistry 61 (2015) 221–230.
[52] Y. Li, et al., Circular RNA is enriched and stable in exosomes: a promising biomarker for cancer diagnosis, Cell Research 25 (2015) 981–984.
[53] W.W. Dong, H.M. Li, X.R. Qing, D.H. Huang, H.G. Li, Identification and characterization of human testis derived circular RNAs and their existence in seminal plasma, Scientific Reports 6 (2016) 39080.
[54] X. Wang, Z. Ding, J. Wu, S. Wang, Y. Zou, Circular RNA in cardiovascular disease, Non-coding. RNA Investig. 1 (2017) 5.
[55] H. Liu, L. Tang, Mechano-regulation of alternative splicing, Current Genomics 14 (2013) 49–55.
[56] J.N. Boeckel, et al., Jumonji domain-containing protein 6 (Jmjd6) is required for angiogenic sprouting and regulates splicing of VEGF-receptor 1, Proceedings of the National Academy of Sciences of the United States of America 108 (2011) 3276–3281.